

Article

Efficient Hydrogenolysis of Guaiacol over Highly Dispersed Ni/MCM-41 Catalyst Combined with HZSM-5

Songbai Qiu, Ying Xu, Yujing Weng, Longlong Ma and Tiejun Wang *

Key Laboratory of Renewable Energy, Guangzhou Institute of Energy Conversion, Chinese Academy of Sciences, Guangzhou 510640, China; qiusb@ms.giec.ac.cn (S.Q.); xuying@ms.giec.ac.cn (Y.X.); wengyj@ms.giec.ac.cn (Y.W.); mall@ms.giec.ac.cn (L.M.)

* Correspondence: wangtj@ms.giec.ac.cn; Tel.: +86-20-8705-7751; Fax: +86-20-8705-7789

Academic Editor: Andreas Martin

Received: 4 July 2016; Accepted: 31 August 2016; Published: 8 September 2016

Abstract: A series of MCM-41 supported Ni catalysts with high metal dispersion was successfully synthesized by simple co-impregnation using proper ethylene glycol (EG). The acquired Ni-based catalysts performed the outstanding hydrogenolysis activity of guaiacol. The effects of the synthesis parameters including drying temperature, calcination temperature, and metal loading on the physical properties of NiO nanoparticles were investigated through the use of X-ray diffraction (XRD). The drying temperature was found to significantly influence the particle sizes of NiO supported on MCM-41, but the calcination temperature and metal loading had less influence. Interestingly, the small particle size (≤ 3.3 nm) and the high dispersion of NiO particles were also obtained for co-impregnation on the mixed support (MCM-41:HZSM-5 = 1:1), similar to that on the single MCM-41 support, leading to excellent hydrogenation activity at low temperature. The guaiacol conversion could reach 97.9% at 150 °C, and the catalytic activity was comparative with that of noble metal catalysts. The hydrodeoxygenation (HDO) performance was also promoted by the introduction of acidic HZSM-5 zeolite and an 84.1% yield of cyclohexane at 240 °C was achieved. These findings demonstrate potential applications for the future in promoting and improving industrial catalyst performance.

Keywords: Ni/MCM-41; HZSM-5; co-impregnation; hydrogenolysis; guaiacol

1. Introduction

In the chemical industry, supported metal catalysts, as the most widely used heterogeneous catalysts, have attracted extensive research [1]. In order to obtain highly active heterogeneous catalysts, active metal components usually need to be loaded on the support materials with high specific surface area. To this purpose, highly ordered mesoporous materials have displayed extensive potential applications in purification and catalysis. Among them, siliceous MCM-41 is regarded as an ideal support for supported metal catalysts due to its large surface area and high porosity, which is able to well disperse the active phase on the surface [2,3]. In order to synthesize Ni-based catalysts with high performance, there are several preparation methods to produce MCM-41 supported Ni catalysts, such as deposition precipitation [4], impregnation [5], ion-exchange [6], in situ incorporation [7], chemical vapor or atomic layer deposition [8], etc. In consideration of the simplicity and practicability of the loading-mode catalyst preparations, the most common method is the use of impregnation using aqueous solutions of nickel salts, such as nickel nitrate [9]. Unfortunately, even at nickel loading below 10 wt %, the use of conventional impregnation could result in the appearance of intense NiO XRD reflections after calcination, indicating the formation of large NiO particles [1,5]. Based on pioneering research work [1,9–13], we have disclosed one simple and practical co-impregnation method using

polyols such as ethylene glycol (EG) to produce MCM-41 supported Ni catalysts with high activity, combining both unprecedentedly high Ni loadings and dispersions [14,15].

Currently, the research and the applications of biofuels derived from biomass have gained great attention, on account of environmental pollution and greenhouse effects [16–18]. The most notable feature of biomass materials is the high oxygen content, and their transformation into hydrocarbon fuels requires deoxygenation through catalytic HDO reactions [19,20]. For the purpose of evaluating the performance of the HDO catalysts, biomass-derived model compounds such as guaiacol have commonly been used in screening and testing the catalytic HDO properties [21,22]. Most of the HDO catalysts combine active metals with various supports, such as Mo-based sulfide catalysts, Ni-based catalysts, noble metal catalysts supported on Al_2O_3 , zeolites, $\text{Al}_2\text{O}_3\text{-SiO}_2$, activated carbon [21–24], and others. Generally, the bifunctional catalytic systems containing a hydrogenating metallic phase and a dehydrating acid phase were preferred to form hydrocarbons [22]. Although the pure siliceous MCM-41 exhibits attractive features such as high specific surface areas and tunable pore sizes, it is lacking in acidic sites, which has restricted its broad applications in catalysis. Thus, it is greatly advantageous to expand the applications of MCM-41 through blending with other suitable zeolites, such as HZSM-5, in order to adjust the quantity of the Brønsted acidity [25,26]. Comparatively, the HDO activity of supported metal catalysts could be clearly improved by the introduction of additional acid sites. Remarkable synergistic effects between metal function and acid sites of the HZSM-5 supported Ni catalyst were revealed, which contributed to the prominent enhancement of the reaction rate in hydrogenation and hydrogenolysis [27]. The product selectivity and the reaction mechanism of guaiacol conversion are mainly subject to the properties of the supports and active metals [28].

In this paper, highly active Ni catalysts supported on MCM-41 were synthesized by co-impregnation with EG, and the synthesis parameters including drying temperature, calcination temperature, and Ni loading were also investigated. Catalytic hydrogenolysis of guaiacol is often considered to be the criterion for evaluating the hydrogenation and HDO activity of supported nickel catalysts, which is of commercial importance in the bio-oil hydro-refining industry [22]. For the purpose of probing the influences of preparation methods and additional introduction of HZSM-5 upon the catalytic properties of Ni/MCM-41, guaiacol hydrogenolysis was used for the catalytic test.

2. Results and Discussion

2.1. Catalyst Characterization

Ni-based samples supported on MCM-41 and HZSM-5 were shortened to Ni/M and Ni/H, respectively. The MCM-41 supported Ni catalysts could be denoted as Ni/M xEG (molar ratio of Ni/EG was 1:x); when x equaled zero, it expressed that the catalysts were prepared by conventional wetness impregnation without EG promotion. The Ni/M(H) 1EG catalyst was prepared by co-impregnation after mixing MCM-41 with 50 wt % HZSM-5 by milling. The synthesis parameters such as drying temperature, calcination temperature, and Ni loading, which influenced the physical properties of the NiO nanoparticles, were investigated through the use of X-ray diffraction (XRD) in Figure 1. In the diffraction patterns of the Ni/M catalysts, the broad and diffuse pattern observed clearly at around $2\theta = 22.5^\circ$ was attributed to amorphous silica. The samples showed diffraction lines at 37.2° , 43.2° , 62.8° , 75.3° , and 79.3° , indicating that nickel was present mainly in the form of the NiO structure after calcination. It was clear that it was pure cubic NiO (JCPDS #00-044-1159).

Figure 1A shows the influence of drying temperature upon the physical properties of the NiO nanoparticles using the XRD technique. The calcination process was kept the same at 400°C for 2 h in air with a heating rate of $2^\circ\text{C}/\text{min}$. The drying temperature varied from 100°C to 200°C and had a clear impact on the particle size and distribution. The samples dried below 120°C had low and diffuse peaks, confirming that extremely small NiO particles were formed and were well dispersed on the MCM-41 support; however, the samples with drying temperatures above 160°C had slightly strong and sharp peaks, which meant that the size of NiO particles grew. The average crystal sizes of NiO increased

gradually from 3.3 nm to 8.0 nm with an increase of the drying temperature from 100 to 200 °C. For the sample dried at 200 °C, it is important to note that there were two types of diffraction peaks on one kind of superimposed diffraction peak; sharp and broad peaks, which indicated two classes of NiO particles with small and large sizes. This showed that very high drying temperatures had a negative effect on the relatively homogeneous particle sizes. The effect of the drying temperature was caused by the boiling point of EG (197.3 °C). When the drying temperature approached or exceeded the boiling point of EG, the EG gradually evaporated and the amount of EG decreased substantially during the drying process. Earlier research revealed that the molar ratio of Ni/EG plays a vital role in controlling the particle sizes and dispersion of NiO on the MCM-41 support [14]. Upon solvent evaporation at a high drying temperature, the residual amount of EG could not inhibit redistribution of the metal salt solution on the surface of the carriers, resulting in the NiO particle growth.

Figure 1B displays the diffraction patterns of 20 wt % Ni/M 1EG samples calcinated at different temperatures after dried at 100 °C. The calcination temperatures had a minor impact on the particle size and distribution. The diffraction peaks of NiO could not emerge at 120 °C, due to the fact that no precursor decomposed to form the NiO crystal structure. After calcination over 150 °C, the peak intensities of NiO were very low and broad. Upon raising the calcination temperature from 550 °C to 800 °C, the Ni/M 1EG samples clearly expressed the broad and diffuse patterns of NiO with average particle sizes below 4.4 nm. This indicated that the Ni-based catalysts had favorable resistance to high temperature sintering by co-impregnation with EG. Generally, as the calcination temperature increased, the particles easily agglomerated and grew larger when using conventional wet impregnation. Thus, the Ni-based catalysts prepared by co-impregnation exhibited a wide temperature window of calcination and excellent resistance to metal sintering due to the strong metal-support interaction [29].

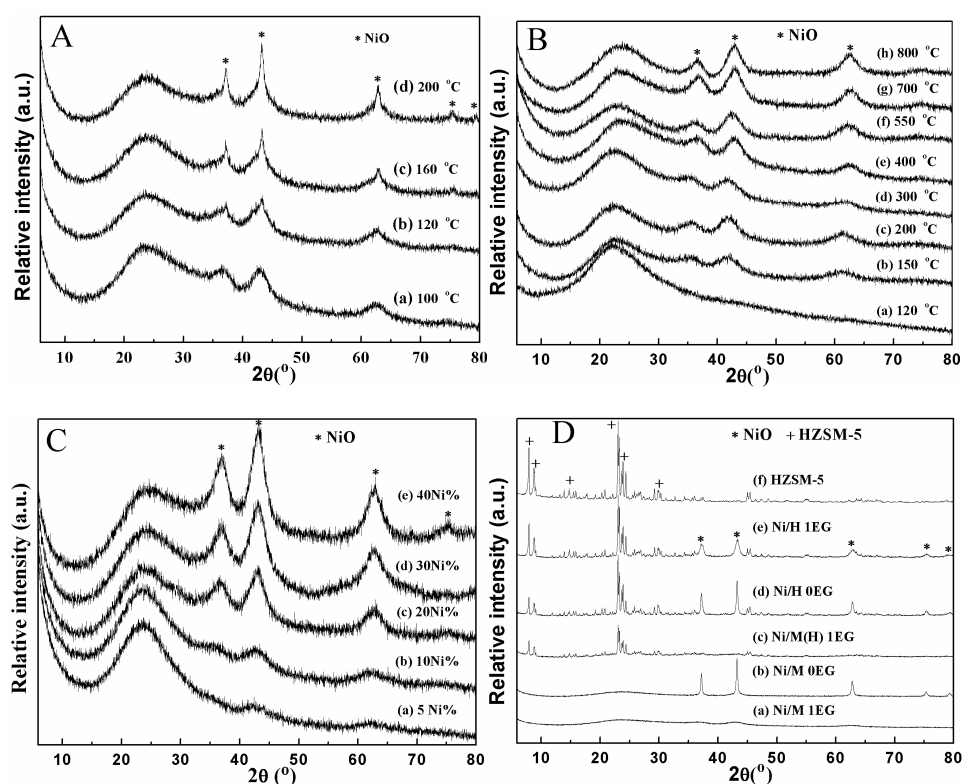


Figure 1. The effects of the synthesis parameters on the XRD patterns of various samples: (A) drying temperature; (B) calcination temperature (20 wt % Ni/M) and (C) Ni loading (5–40 wt % Ni/M) during co-impregnation with Ni/EG = 1:1; (D) 20 wt % Ni catalysts on different supports including MCM-41 and HZSM-5.

Figure 1C exhibits the XRD profiles of the Ni/M 1EG samples with different Ni loading varying from 5–40 wt % by co-impregnation. The diffraction intensity of the 5 wt % Ni/M 1EG sample was too low to be analyzed, implying that the smaller particle size of NiO (<3.3 nm) was formed on the support due to its higher dispersion. When the metal loading exceeded 5 wt %, new dispersive diffraction patterns appeared. The diffraction peak intensity of the samples gradually increased as the metal content increased. According to the above results, NiO could be better dispersed on the MCM-41 surface using co-impregnation, and superfine NiO nanoparticles below 3.7 nm could be produced until the metal loading amount was 40 wt %. This clearly showed that the EG added during impregnation had a sufficient ability to control the relatively homogeneous particle sizes and the high dispersion for excess metal loading. This might be caused by the large surface area of the MCM-41 support, which could support excess metal even with 40 wt % Ni loading.

The pure siliceous MCM-41 lacks acidic sites, which restricts its broad application in catalysis. For the hydrorefining of bio-oil, bifunctional catalysts containing a hydrogenating metallic phase and a dehydrating acid phase are preferred to form hydrocarbons [21,22]. Thus, it was particularly useful that the quantity and distribution of acidic sites on the catalyst supports containing MCM-41 was modified and improved by the strong acidity of other zeolites, such as HZSM-5. As shown in Figure 1D, the Ni-based samples supported on MCM-41 and HZSM-5 were also investigated by XRD analysis. Typical diffraction peaks for the HZSM-5 crystalline phase centered at $2\theta = 7.9^\circ$, 8.7° , 23.0° , and 23.9° were observed. The average crystal sizes of NiO supported on HZSM-5 decreased to 13.3 nm from 42.9 nm after co-impregnation with EG. In particular, the XRD patterns of Ni/M(H) 1EG also exhibited very low intensities and dissemination of the NiO diffraction peaks, suggesting that the mixed carrier containing MCM-41 and HZSM-5 could stabilize and disperse the special small metal particles as well as the single supporter of MCM-41. This could be caused by the high water-absorbing quality of its large pore volume and the high specific surface area of the MCM-41 support, resulting in the preferential adsorption of the impregnation solution by the MCM-41 in the mixed supports (Figure 2D and Figure S1). Consequently, the catalyst of Ni/M(H) 1EG not only retained the high hydrogenation activity of the Ni metallic phase, but also possessed the corresponding amount of dehydrating acidic sites.

The TEM images of the Ni-based samples are shown in Figure 2A–D. Compared with conventional wetness impregnation, co-impregnation avoided NiO aggregation into even larger clusters on the MCM-41 support surface and facilitated the formation of remarkably smaller NiO particle sizes. A similar trend was observed on the HZSM-5 support. Particularly, NiO particles on the mixed supports containing MCM-41 and HZSM-5 were comparatively dispersed compared to the single MCM-41 support (Figure S1). Table 1 summarizes the physicochemical and structural parameters of the various samples. After impregnation, the Brunauer-Emmett-Teller (BET) specific surface area clearly decreased, as well as the total pore volume. The drop in porosity and specific surface area might be ascribed to the formation of blockages on the support surface and channels. This indicated that the procedure of preparing the catalysts had no severe impact upon the molecular sieve structures and the order channels of HZSM-5 and MCM-41 (Figure S2).

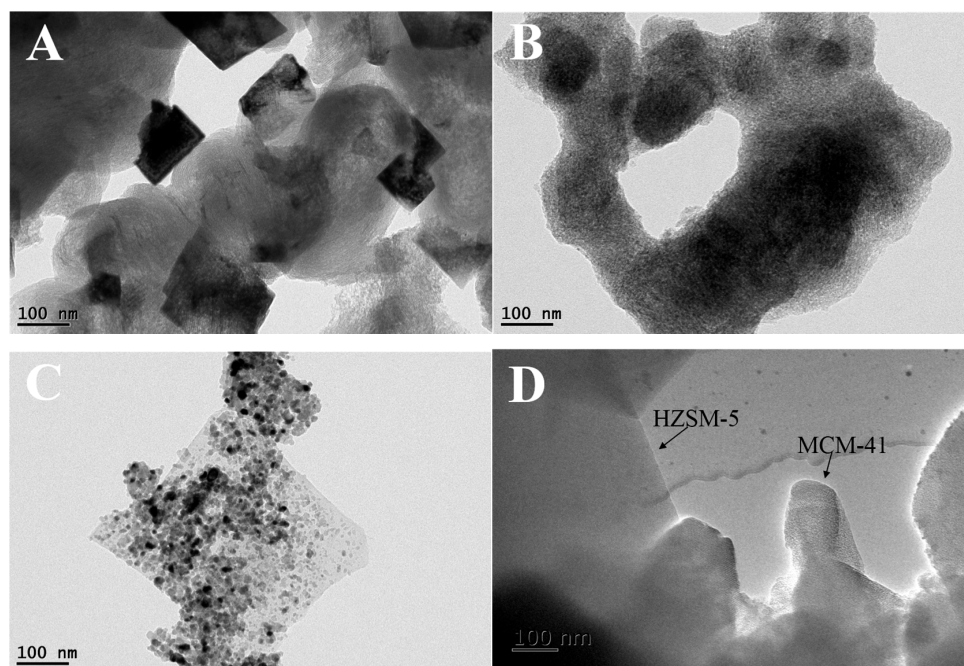


Figure 2. The TEM pictures of the synthesized samples (20 wt % Ni loading): (A) Ni/M 0EG; (B) Ni/M 1EG; (C) Ni/H 1EG; and (D) Ni/M(H) 1EG.

As illustrated in Figure 3 and Table S1, H₂ temperature-programmed reduction (H₂-TPR) experiments were performed to analyze the reducibility and reduction degrees of the Ni-based catalysts. The H₂ consumption peak around 300–400 °C was associated with the reduction of bulk nickel oxide [5,28–30]. On the other hand, the reduction peak at higher temperatures (>500 °C) could be related to the reduction of nickel oxide species, which strongly interacted with the support and appeared to be difficult to reduce [4,5,31,32]. In comparison with the Ni/M 0EG catalyst, the Ni/M 1EG catalyst was quite different in reduction performance. The H₂ consumption peaks were very broad, and shifted to higher temperature. According to the above results, we could consider that the existence of the nickel oxide species that were difficult to reduce was caused by the strong metal-support interaction using co-impregnation. In the case of Ni/H 1EG, the H₂-TPR profile exhibited one strong and sharp peak at around 310 °C, which showed that the reduction of NiO species relied heavily upon the nature of the support. Therefore, we can reasonably speculate that the main peak shift to 520 °C of the Ni/M(H) 1EG catalyst from 610 °C of the Ni/M 1EG catalyst was caused by the weaker interaction between the NiO and the HZSM-5 support. After reduction at 450 °C in H₂ flowing for 4 h, the new diffraction peaks of Ni appeared, and the metal Ni kept the approximate crystal sizes and dispersion of NiO (Figure S3).

Table 1. Physicochemical characteristics of the samples.

Samples ^a	Mole Ratio Ni:EG	S _{BET} (m ² /g) ^b	Pore Volume (cm ³ /g) ^b	Average Pore Diameter (nm) ^b	Mean Particle Size Diameter (nm) ^c
MCM-41	-	1063	1.12	2.8	-
Ni/M 0EG	1:0	807	0.67	2.7	45.0
Ni/M 1EG	1:1	785	0.70	2.8	3.3
HZSM-5	-	420	0.21	3.7	-
Ni/H 0EG	1:0	231	0.09	3.7	42.9
Ni/H 1EG	1:1	216	0.06	3.6	13.3
Ni/M(H) 1EG	1:1	510	0.42	2.9	<3.0

^a Metal loading of the Ni-based catalysts was kept at 20 wt %; ^b Obtained from BET and BJH equations, respectively; ^c Calculated with the Scherrer equation from the XRD pattern at 2θ = 43.3°.

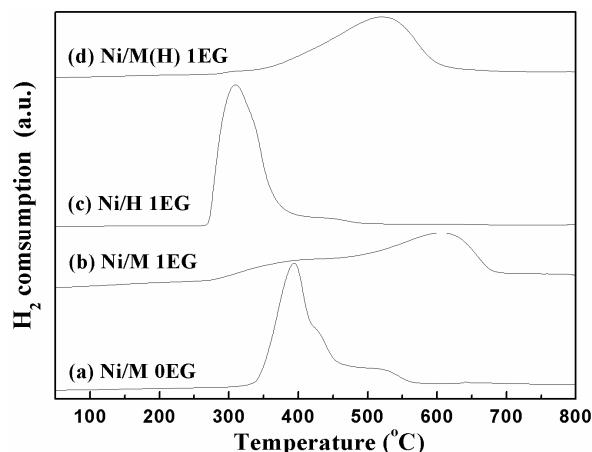


Figure 3. H₂ temperature-programmed reduction (H₂-TPR) of different samples with 20 wt % Ni loading.

XPS analysis was also performed to investigate the oxidation states of Ni at the outer layers of the various samples in Figure 4. Generally, the binding energy of Ni-2p_{3/2} in the metallic Ni was about 852.4 eV [33,34]. It was unambiguous that there was no metallic Ni present on the samples before reduction. The shoulder peak at 854–857 eV and the broad satellite centered at about 861.6 eV clearly indicated the presence of NiO [34,35]. By comparison of the relevant binding energies with the observed Ni-2p_{3/2} satellite separation, it was determined that NiSiO_x species were not formed over all the catalysts [35]. The broad Ni-2p_{3/2} profiles could be deconvoluted into two components, which indicated that there were two kinds of NiO species formed on the carrier surface. The peaks at around 854.5 and 856.4 eV were assigned to Ni²⁺ in bulk NiO and small NiO particles, respectively, corresponding to weak and strong interaction with the supports [36,37]. The Ni-2p binding energy shift could be essentially explained by the particle size effect, in which the small NiO particles easily caused a charge transfer from NiO clusters to the support substrates, resulting in the strong metal-support interaction and the presence of NiO species that were difficult to reduce [37]. Moreover, the surface area ratio of the two Ni-2p_{3/2} peaks elucidated the component proportion of weak and strong interactions, which was in agreement with the H₂-TPR results described above.

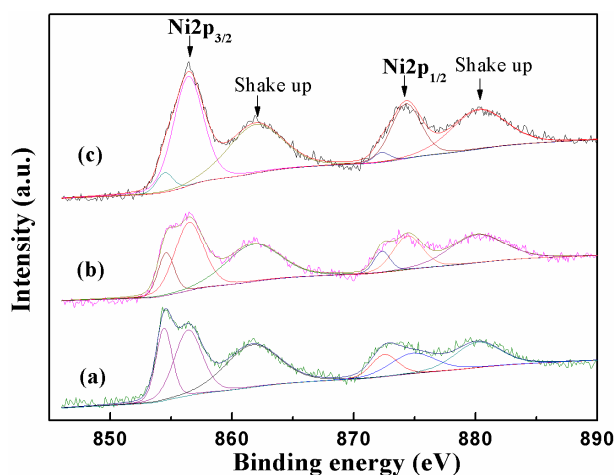


Figure 4. Ni-2p region of the XPS spectra of various samples without reduction (20 wt % Ni loading): (a) Ni/M 0EG; (b) Ni/M 1EG and (c) Ni/M(H) 1EG.

To characterize the overall concentration and strength of the acid sites on various samples, temperature-programmed desorption of ammonia (NH_3 -TPD) analysis was performed. The NH_3 -TPD spectrum of the tested samples displayed a broad distribution of acid sites with weak and strong strength, shown in Figure 5, and the quantitative data of NH_3 adsorbed for the various samples are shown in Table 2. The low-temperature desorption peak at around 250 °C could correspond to NH_3 adsorbed on the weak acid sites derived from surface silanol groups. As expected, the high-temperature peak at about 467 °C suggested the presence of strong acid sites associating with Al-OH and Al-OH-Si groups in the HZSM-5 surface and structure [38,39]. Nevertheless, for the Ni/M 1EG sample, there was only one very weak desorption peak that appeared at approximately 192 °C, suggesting purely siliceous MCM-41 was short of acid sites [40]. After Ni impregnation of the HZSM-5 support, the acid amount was slightly less than that of HZSM-5 with the exception of a strong desorption peak shift to higher temperature; the temperature of the weak desorption peaks was almost unchanged, indicating that the loading of Ni mainly changed strong acid sites [41]. Particularly, the distribution and strength of the acid sites had been changed significantly after the additional introduction of MCM-41 into the Ni/HZSM-5 1EG sample. The amount of strong acid obviously decreased, and a distinct shift of the desorption peak of the weak acid sites towards lower temperatures was observed. Normally, Brønsted acidity was ascribed to acid sites with a desorption temperature above 300 °C [42]. Based on the NH_3 -TPD studies, it could be considered that the quantity of Brønsted acid sites in HZSM-5 significantly declined after mixing with MCM-41, which was well consistent with the previous reports [25]. The framework Al in HZSM-5 zeolite could be extracted by the silicon species in the framework of MCM-41, leading to the acidity adjustment of mixed zeolites. According to pyridine-adsorbed infrared spectroscopy in the literature, it is convincing evidence of the main existence of Brønsted acidic sites in addition to small amounts of Lewis acidic sites due to the reinforced interaction between HZSM-5 and MCM-41 when the two supports were mixed [25]. Generally, the selective hydrogenolysis of C–O and C–C bonds was strongly dependent on the acidic properties of the catalyst supports; therefore, the weak-acid sites were conducive to the dehydration reaction in the C–O hydrogenolysis while the strong-acid sites often caused the rupture of C–C bonds. Thus, the concentration and properties of acidic sites on the mixed carrier could be regulated by mixing MCM-41 with HZSM-5, which would be beneficial for the improvement of C–O hydrogenolysis.

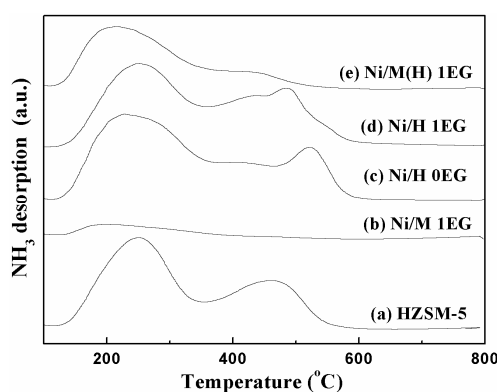


Figure 5. Ammonia desorption profiles from various samples without reduction (20 wt % Ni loading).

Table 2. NH_3 -TPD results of various Ni catalysts with 20 wt % Ni loading.

Catalyst	Peak Position (°C)		Acid Amount (umol/g)		
	T1	T2	Total	Weak	Strong
HZSM-5	250	467	622	414	208
Ni/H 0EG	253	508	550	372	178
Ni/H 1EG	252	485	492	328	164
Ni/M 1EG	192	-	87	87	0
Ni/M(H) 1EG	212	412	350	309	41

2.2. Guaiacol Hydrogenolysis Activity of Prepared Catalysts

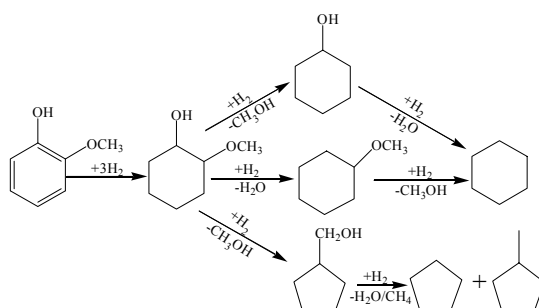
To explore the hydrogenolysis activity of various catalysts prepared by co-impregnation, the Ni-based catalysts were comparatively investigated in the hydrogenation and HDO of guaiacol at different temperatures, respectively shown in Tables 3–5. The 20 wt. % Ni loading was determined to be selected as proper metal loading for the following tests (Table S2). The results coincide well with the hydrogenolysis mechanism on noble metal catalysts that comprise the hydrogenation saturation of a benzene ring preferentially and the HDO of oxygenates after hydrogenation in the successive step [22,28] (Scheme 1). The main products of low temperature hydrogenation below 200 °C were methoxycyclohexanol, apart from a small amount of cyclohexanol, methoxycyclohexane, and cyclohexane. In respect to various Ni-based catalysts prepared using impregnation and co-impregnation, the hydrogenation activity below 200 °C was observed to have the following trend (Table 3):

Hydrogenation activity: Ni/M (H) 1EG \approx Ni/M 1EG > Ni/M 1EG + H > Ni/M 0EG > Ni/H 1EG.

Table 3. Hydrogenation activity of guaiacol on various catalysts under low temperature ^a.

Catalyst	Temp. °C	X _{GUA} %	S _{Methoxycyclohexanol} %	S _{Cyclohexanol} %	S _{Methoxycyclohexane} %	S _{Cyclohexane} % ^b
Ni/M 0EG	150	15.5	96.3	1.8	0	0.4
Ni/M 0EG	200	92.6	91.1	5.1	0.5	1.3
Ni/M 1EG	100	12.3	94.4	5.6	0	0
Ni/M 1EG	120	34.8	93.0	6.4	0.4	0.2
Ni/M 1EG	150	97.4	93.9	5.3	0.5	0.2
Ni/M 1EG	200	100	89.7	5.9	1.1	2.1
Ni/H 1EG	200	14.4	89.5	2.7	0.7	3.5
5% Pd/C	100	18.1	97.0	1.8	0.9	0.3
5% Pd/C	120	61.7	97.4	2.3	0.3	0
5% Pd/C	150	100	97.8	1.4	0.7	0
5% Ru/C	100	83.4	82.8	16.1	0.1	0
5% Ru/C	120	92.3	82.3	15.8	1.0	0
5% Ru/C	150	100	71.3	25.8	0.9	0
Ni/M 1EG +H	150	87.3	93.6	4.4	0.3	0.9
Ni/M 1EG +H	200	100	66.5	29.2	2.1	2.2
Ni/M (H) 1EG	120	45.1	90.6	8.2	0.6	0.3
Ni/M (H) 1EG	150	97.9	94.1	4.5	0.5	0.5
Ni/M (H) 1EG	200	100	75.4	1.9	2.1	15.9

^a Reaction conditions: 1.0 g guaiacol, 9.0 g *n*-dodecane (solvent), 0.15 g Ni-based catalysts, 0.15 g commercial 5 wt % Pd/C and Ru/C catalyst, 120–200 °C, 5.0 MPa (ambient temperature), 1000 rpm/min, 120 min. For Ni/M 1EG +H, 0.15g Ni/M 1EG catalyst with additional solid acid of 0.12 g HZSM-5; ^b There were some other products that mainly included 1,2-cyclohexanediol, 1,2-dimethoxycyclohexane, methylcyclopentane, and cyclopentane, etc.



Scheme 1. Proposed main reaction pathways for the conversion of guaiacol with hydrogenation and deoxygenation on highly dispersed Ni/MCM-41 catalysts combined with HZSM-5.

In comparison with the Ni/M 0EG catalyst prepared by conventional wetness impregnation, the Ni/M 1EG prepared via co-impregnation presented outstanding catalytic activity in the guaiacol

hydrogenation. For example, the guaiacol conversion of Ni/M 0EG increased from 15.5% to 92.6% when the reaction temperature increased from 150 to 200 °C. Correspondingly, on the Ni/M 1EG catalyst, the guaiacol conversion reached 97.4% at 150 °C. Even at 100 °C, there was 12.3% guaiacol conversion. Compared with the commercial 5% Pd/C and 5% Ru/C catalysts (Aladdin Reagents (Shanghai) Co., Ltd., Shanghai, China), the Ni/M 1EG catalyst prepared by co-impregnation exhibited similar activity with noble metal catalysts in the guaiacol hydrogenation. Thus, the catalytic activity of Ni-based catalysts supported on MCM-41 could be strongly enhanced by co-impregnation, which was essentially attributed to the high dispersion and ultra-small size of the NiO nanoparticles. Although the Ni/H 1EG catalyst had a mean NiO particle size of about 13.3 nm, it unexpectedly performed with poor hydrogenation activity, which was much lower than that of the Ni/M 1EG sample. For supported metal catalysts, it is well known that the hydrogenolysis activity of guaiacol is significantly dependent on the physicochemical properties of the support materials. The microporous HZSM-5 support presented not only the small pore volume but also the low special surface area. Moreover, the 20 wt % Ni loading dispersed on the HZSM-5 support led to the further decrease of the BET specific surface area and the blocking of the pore-channel structure. Conversely, the MCM-41 support had a high specific surface area, large pore volumes, and homogeneous hexagonal mesopore arrays, resulting in more adsorption and enrichment of the guaiacol reactant on the catalyst surface [25,43]. Consequently, on the HZSM-5 support, this insufficient enrichment of guaiacol may be the cause of the low hydrogenation activity.

In addition, it is widely known that the surface acidity of solid catalysts plays a crucial role in catalytic HDO reactions. In order to improve the HDO performance of the Ni/M 1EG catalyst, the quantity of Brønsted acidity of the MCM-41 support was enhanced by additional introduction of HZSM-5. However, the guaiacol conversion decreased to 87.3% from 97.4% at 150 °C using the Ni/M 1EG catalyst together with the addition of a given mass of HZSM-5. This decreased activity could be explained by blocking of the hydrogenation active sites through coverage of the surface of the Ni/M 1EG catalyst with additional HZSM-5. Fortunately, the Ni/M(H) 1EG catalyst kept the comparative hydrogenation activity at low temperature. This was consistent with the XRD and TEM results, indicating that super small and highly dispersed NiO nanoparticles on the mixed supports containing MCM-41 and HZSM-5 also had outstanding hydrogenation activity.

Table 4. Hydrodeoxygenation activity of guaiacol on various catalysts under high temperature ^a.

Catalyst	Ni/M 0EG			Ni/M 1EG			Ni/H 1EG ^b			
	Temp. (°C)	220	240	250	220	240	250	220	250	280
S _{Methoxycyclohexanol}	81.2	56.9	29.1	78.3	29.7	0.2	74.4	50.9	0.1	
S _{Cyclohexanol}	6.1	5.6	3.8	6.5	4.6	0	3.7	1.3	0	
S _{Methoxycyclohexane}	1.3	0	3.9	1.9	5.0	0	1.6	0.8	0	
S _{Methylolcyclopentane}	3.7	10.1	12.7	3.2	5.6	0	0.4	0.6	0	
S _{Cyclohexane}	6.6	25.5	44.8	9.0	43.4	73.0	12.9	39.6	85.4	
S _{Methylcyclopentane}	0	0.3	0.7	0	0.5	1.3	1.4	4.0	9.2	
S _{Cyclopentane} ^c	0.1	1.2	4.6	0.5	10.7	25.2	0.5	0.3	1.1	

^a Reaction conditions: 1.0 g guaiacol, 9.0 g *n*-dodecane (solvent), 0.15 g Ni-based catalysts, 220–280 °C, 5.0 MPa (ambient temperature), 1000 rpm/min, 120 min; ^b For the Ni/H 1EG catalyst, the conversions of guaiacol at 220 °C, 250 °C, and 280 °C were 33.7%, 67.6% and 98.7%, respectively. Other catalysts showed the full conversion at temperatures up to 200 °C; ^c There were some other products mainly included *n*-hexane, *n*-pentane, methylcyclohexane, methylcyclopentane, butane, and others.

The results presented above demonstrated that the distribution of products expressed a clear dependence on the reaction temperature. The HDO of oxygenated products originating from hydrogenation of the benzene ring mainly took place in the temperature range of 220–280 °C on these Ni-based catalysts. The formation of alkane products was usually considered to dissociate C–O bonds by demethoxylation and dehydroxylation [44]. The detectable HDO products were mainly comprised of cyclohexane, methylcyclopentane, cyclopentane, methylolcyclopentane, methoxycyclohexane, and

cyclohexanol. The following trend of HDO activity above 220 °C was revealed over various Ni-based catalysts (Tables 4 and 5):

HDO activity: Ni/M (H) 1EG \approx Ni/M 1EG +H > Ni/M 1EG > Ni/M 0EG > Ni/H 1EG.

Table 5. Hydrodeoxygenation activity of guaiacol promoted by HZSM-5 under high temperature ^a.

Catalyst ^b	Ni/M 1EG+H ^c			Ni/M(H) 1EG			
	Temp. (°C)	220	240	250	220	240	250
S _{Methoxycyclohexanol}		26.7	3.0	0	34.0	0	0.3
S _{Cyclohexanol}		1.5	0.3	0	2.0	0	0
S _{Methoxycyclohexane}		4.2	1.2	0	4.7	0	0
S _{Methylolcyclopentane}		10.6	3.2	0	7.8	0	0
S _{Cyclohexane}		52.0	82.0	88.4	45.1	84.1	84.2
S _{Methylcyclopentane}		1.9	4.6	5.8	1.5	4.8	5.4
S _{Cyclopentane} ^d		2.7	4.9	4.6	4.2	10.3	8.9

^a Reaction conditions: 1.0 g guaiacol, 9.0 g *n*-dodecane (solvent), 0.15 g Ni-based catalysts, 220–280 °C, 5.0 MPa (ambient temperature), 1000 rpm/min, 120 min. For Ni/M 1EG +H, 0.15 g Ni/M 1EG catalyst with additional solid acid of 0.12 g HZSM-5; ^b Two catalysts also showed the full conversion at temperatures up to 200 °C; ^c For Ni/M 1EG +H, 0.15g Ni/M 1EG catalyst with additional solid acid of 0.12 g HZSM-5; ^d There were some other products which mainly included *n*-hexane, *n*-pentane, methylcyclohexane, methylpentane, butane, and others.

Moreover, the very small and highly dispersed NiO nanoparticles on the MCM-41 supports prepared by co-impregnation exhibited the higher HDO activity. However, the Ni/H 1EG catalyst presented both poor hydrogenation and HDO activity. For the Ni/H 1EG catalyst, the conversions of guaiacol at 220 °C, 250 °C, and 280 °C were 33.7%, 67.6%, and 98.7%, respectively. Correspondingly, other catalysts showed the full conversion at temperatures up to 200 °C. The yield of cyclohexane was increased to 73.0% on the Ni/M 1EG catalyst from 44.8% on the Ni/M 0EG catalyst at 250 °C. Obviously, the HDO activity of the Ni/M 1EG catalyst for guaiacol hydrogenolysis to cyclohexane was significantly enhanced by the addition of HZSM-5. The cyclohexane yield was rapidly raised to 52.0% from 2.2% by elevating the reaction temperature from 200 °C to 220 °C. Generally, the surface acids of heterogeneous catalysts could accelerate the breakage of C–O bonds by promoting dehydration in HDO reactions; therefore, many reaction systems adopted an acid as an efficient component in the catalysts. The cooperation between the hydrogenating metal sites and the dehydrating acidic sites could be responsible for obtaining the excellent HDO activities [22]. Similar to the mechanical mixed catalyst of Ni/M 1EG+ H, the Ni/M(H) 1EG catalyst kept the comparative HDO activity at high temperature. Undoubtedly, this proved that the HDO reaction activity could be distinctly improved by strengthening the surface acid intensity of the catalyst supports. During the experiment, it was found that the selectivity for methoxycyclohexanol displayed an opposite trend with the increasing reaction temperature, which was caused by the C–O bond dissociations by both demethoxylation and dehydroxylation [29]. Particularly, 84.1% yield of cyclohexane on the Ni/M(H) 1EG catalyst was achieved at 240 °C. Main byproducts were methylcyclopentane and cyclopentane, accompanied by a small amount of methyl-cyclohexane, *n*-hexane, *n*-pentane, methylpentane, butane, etc. It was noted that some guaiacol conversion schemes reported in the literature also included transalkylation reactions, isomerization reactions, ring-opening reactions, and C–C bond dissociations, which were responsible for the detected byproducts [30,45].

In summary, well-dispersed nickel species on MCM-41 supports played a key role in both guaiacol conversion and hydrogenolysis performance, and the Ni/M 1EG catalyst synthesized using co-impregnation exhibited much higher hydrogenation and HDO activity in comparison with that of the Ni/M 0EG sample using conventional impregnation. The NiO supported on the mixed supports containing MCM-41 and HZSM-5 not only maintained the high dispersion, but also kept the comparative hydrogenation activity with noble metal catalysts at low temperature. Moreover, the HDO activity at high temperatures could be clearly improved by the introduction of

HZSM-5 zeolite. Acid sites could promote demethoxylation and rearrangement of the intermediate methoxycyclohexanol. Obvious synergistic effects between the Brønsted acidic sites of supports and metallic Ni active phases were observed, which contributed to the prominent enhancement of the reaction rate in HDO of guaiacol (Table S3, Figure S4 and Figure S5). Meanwhile, larger BET surface area and homogeneous mesopores of MCM-41 facilitated the adsorption of guaiacol and hydrogen molecules on the catalysts, and favored the reactants' collision, which improved the efficiency of the guaiacol hydrogenation. Therefore, one bifunctional catalyst of Ni/M(H) 1EG could be easily achieved by co-impregnation and mechanical mixing of MCM-41 and HZSM-5, and it could present higher HDO activity of guaiacol by the combination of metal-catalyzed hydrogenation and acid-catalyzed C–O bond dissociations. The observations above indicated that the hydrogenolysis of guaiacol occurred through the reaction pathway in which the hydrogenation saturation of the aromatic ring was performed to form methoxycyclohexanol as the first step, and was subsequently hydrodeoxygenated to generate cyclohexane. Consequently, the Ni/M(H) 1EG catalyst possessed similar activity with noble metal catalysts in the guaiacol hydrogenation, and it exhibited not only higher hydrogenation activity at low temperatures, with a 97.9% guaiacol conversion at 150 °C, but high HDO activity at high temperature, with an 84.1% yield of cyclohexane (C1-based) at 240 °C. In summary, this study could contribute to the development and improvement of supported metal catalysts applied in the chemical industry.

3. Experimental Section

3.1. Catalyst Preparation

Molecular sieves (pure siliceous MCM-41 and HZSM-5 with Si/Al molar ratio of 38) were selected as support materials and were supplied by The Catalyst Plant of Nankai University (Tianjin, China). Ni/MCM-41 (shortened to Ni/M) and Ni/HZSM-5 (shortened to Ni/H) catalysts with 20.0 wt % Ni loading were synthesized using conventional wetness impregnation and co-impregnation according to an established procedure [14]. First, an appropriate amount of carriers were impregnated using the proper nickel nitrate solution ($\text{Ni}(\text{NO}_3)_2 \cdot 6\text{H}_2\text{O}$ was purchased from Aladdin Reagents (Shanghai) Co., Ltd., Shanghai, China) and were kept standing for 12 h. Subsequently, the wet sample was dried by stirring in air at 100 °C overnight. Then, the dried sample was placed in a muffle furnace, and the furnace temperature was gradually raised to 400 °C with a heating rate of 2 °C/min. Finally, the required sample could be obtained after calcination in air atmosphere for 2 h. The preparation process of co-impregnation was the same as that of the conventional wetness impregnation except that it was necessary to add quantitative ethylene glycol (EG) into the nickel nitrate aqueous solution (the molar ratio of Ni/EG was 1:1). The MCM-41 supported Ni catalysts were denoted as Ni/M xEG (the molar ratio of Ni/EG was 1:x); when x equaled zero, it meant that the catalysts were prepared by conventional wetness impregnation without EG promotion. The Ni/M(H) 1EG catalyst was prepared by co-impregnation after mixing MCM-41 with 50 wt % HZSM-5 by milling.

3.2. Catalyst Tests

The hydrogenolysis reaction of guaiacol was performed in a 50 mL stainless-steel batch autoclave. The reaction system was heated with an automatic temperature control device, and the magnetic stirring speed was kept at 1000 rpm using the stir bar. Before hydrogenation, the Ni-based catalysts were reduced at 450 °C in the presence of flowing H_2 for 4 h. For each run, 1.0 g guaiacol (reactant), 9.0 g *n*-dodecane (solvent), and 0.15 g of Ni-based catalysts were placed in the batch autoclave. The initial reaction pressure of hydrogen was sealed at 5 MPa after displacing the air in the autoclave six times using pure H_2 . Subsequently, the reaction temperature was heated to 120–280 °C using a temperature controller. After reaction for 120 min, the autoclave was immediately cooled in an ice-water bath, and the product compositions were taken out for detection by capillary gas chromatography (Shimadzu GC-2010, Shimadzu Corporation, Kyoto, Japan), coupled to a FID detector (hydrogen flame ionization detector), using an AT SE-30 column (50 m length, 0.32 mm inner diameter, 0.33 μm film).

3.3. Catalyst Characterization

The crystalline phase of various samples was identified by X-ray diffraction (XRD) analysis with a X'Pert PRO Philips diffractometer (PANalytical B.V., Almelo, The Netherlands) using Cu K α radiation (0.1541784 nm). The scanning mode was set at a step size of 0.0167° and a step counting time of 10 s in the 2 θ range from 5° to 80° at 298 K. The BET (Brunauer-Emmet-Teller) specific surface area of various samples was tested by nitrogen isothermal adsorption in a Quadrasorb SI system (Quantachrome, Boynton Beach, FL, USA), and determined by a multipoint BET method using the desorption data in the relative pressure (p/p_0) range of 0.05–0.3. The samples could be degassed at 250 °C for 3 h. Pore size distribution and pore volume obtained in this paper were calculated from the N₂ isotherm at 77 K by the BJH method. Transmission electron microscope (TEM) images were recorded using a JEOL JEM-2010 microscope (JEOL Ltd., Tokyo, Japan) with an electron beam of 200 kV. For the TEM observation, the as-prepared samples were dispersed in ethanol by ultrasonic dispersion for about 30 min and were then dropped onto a copper grid. The XPS (X-ray photoelectron spectroscopy) measurements were tested on an ESCALAB 250 spectrometer (Thermo Electron Corp., Altrincham, UK) with an Al K α source (1486.6 eV) and all the binding energies of Ni were calibrated according to the C-1s peak at 284.6 eV. H₂-TPR (hydrogen temperature-programmed reduction) studies were performed on a Micromeritics Autochem apparatus (model 2910, Micromeritics Instrument Co., Norcross, GA, USA) using a TCD detector (thermal conductivity detector). 50 mg of the sample was placed in a quartz tube and pretreated in N₂ atmosphere at 300 °C for 1 h before performing the TPR program. The sample was heated under a 5% H₂/N₂ flow (30 mL/min) at a ramp of 10 °C/min from 50 °C to 950 °C.

4. Conclusions

Highly active Ni-based catalysts supported on MCM-41 or its mixed supports containing HZSM-5 were easily tailored using co-impregnation with EG. The synthesized catalysts performed with comparatively outstanding hydrogenation and HDO activity in the guaiacol hydrogenolysis with noble metal catalysts. The synthesis parameters such as drying temperature, calcination temperature, and nickel loading were carefully studied. Compared to the calcination temperature and nickel loading, the drying temperature exhibited an obvious effect on the resulting particle sizes and dispersion of NiO supported on MCM-41. The strong metal-support interaction led to about 3.3 nm NiO nanoparticle formation, excellent anti-sintering even at 800 °C, and high metal loading with 40 wt %. The highly dispersed nickel species supported on the mixed supports containing MCM-41 and HZSM-5 still exhibited outstanding low-temperature hydrogenation activity with a guaiacol conversion of 97.9% at 150 °C. The HDO efficiency was improved by increasing the acidity amount using additional introduction of HZSM-5 zeolite and the cyclohexane yield of 84.1% was achieved at 240 °C. The observations above indicated that the catalysis progressed through a step-wise and bi-functional mechanism as reported on supported noble metal catalysts where the methoxycyclohexanol was mainly formed by hydrogenation of the aromatic ring in guaiacol as the first step, and subsequently hydrodeoxygenated to generate cyclohexane. The catalytic activity of the supported catalysts by simple co-impregnation was significantly improved, which makes them high attractive for potential applications in the bio-refinery industry.

Supplementary Materials: The following are available online at www.mdpi.com/2073-4344/6/9/134/s1. Table S1: The reduction degrees of the Ni-based catalysts, Table S2: Hydrogenation activity of guaiacol on various catalysts with different Ni loading at 150 °C, Table S3: Hydrogenolysis activity of guaiacol over Ni/M(H) 1EG under different reaction times, Figure S1: TEM pictures of synthesized Ni/M(H) 1EG sample with different electron beam irradiation times (the time is increasing from **A** to **D** photos corresponding to 1min, 3min, 4min and 5min), Figure S2: The XRD patterns of MCM-41 and MCM-41-supported catalysts: (**A**) low-angle XRD patterns; (**B**) high-angle XRD patterns, Figure S3: The XRD patterns of various catalysts before and after reduction (**A**) Ni/M 0EG and (**B**) Ni/M 1EG. Reduction conditions: reduction at 450 °C for 4 h under atmospheric pressure of 100% H₂, Figure S4: GC analysis of the products for guaiacol HDO at 240 °C with different reaction times on Ni/M(H) 1EG, Figure S5: GC analysis of the products for guaiacol HDO at 240 °C for 30 min on Ni/M(H) 1EG and Ni/M 1EG, respectively.

Acknowledgments: This work was financially supported by the National Natural Science Foundation of China (No. 21306195 & 51476176).

Author Contributions: S.Q., X.Y., Y.W., L.M., and T.W. conceived, designed, and discussed the total experimental methods and test results. S.Q. and Y.W. carried out the laboratory experiments and analyzed the data. S.Q. wrote the initial draft and prepared the revised version. All authors discussed the experimental results above and revised the full manuscript.

Conflicts of Interest: The authors declare no conflict of interest.

References

1. Van Dillen, A.J.; Terörde, R.M.; Lensveld, D.J.; Geus, J.W.; de Jong, K.P. Synthesis of supported catalysts by impregnation and drying using aqueous chelated metal complexes. *J. Catal.* **2003**, *216*, 257–264. [[CrossRef](#)]
2. Kresge, C.T.; Leonowicz, M.E.; Roth, W.J.; Vartuli, J.C.; Beck, J.S. Ordered mesoporous molecular sieves synthesized by a liquid-crystal template mechanism. *Nature* **1992**, *359*, 710–712. [[CrossRef](#)]
3. Lopez, L.; Velasco, J.; Montes, V.; Marinas, A.; Cabrera, S.; Boutonnet, M.; Jaras, S. Synthesis of Ethanol from Syngas over Rh/MCM-41 Catalyst: Effect of Water on Product Selectivity. *Catalysts* **2015**, *5*, 1737–1755. [[CrossRef](#)]
4. Nares, R.; Ramirez, J.; Gutierrez-Alejandre, A.; Cuevas, R. Characterization and Hydrogenation Activity of Ni/Si(Al)-MCM-41. Catalysts Prepared by Deposition-Precipitation. *Ind. Eng. Chem. Res.* **2009**, *48*, 1154–1162. [[CrossRef](#)]
5. Lensveld, D.J.; Mesu, J.G.; van Dillen, A.J.; de Jong, K.P. Synthesis and characterization of MCM-41 supported nickel oxide catalysts. *Microporous Mesoporous Mater.* **2001**, *44–45*, 401–407. [[CrossRef](#)]
6. Yonemitsu, M.; Tanaka, Y.; Iwamoto, M. Metal Ion-Planted MCM-41. 1. Planting of Manganese (II) Ion into MCM-41 by a Newly Developed Template-Ion Exchange Method. *Chem. Mater.* **1997**, *9*, 2679–2681. [[CrossRef](#)]
7. Chanquia, C.M.; Winkler, E.L.; Causa, M.T.; Eimer, G.A. Evolution of Copper Nanospecies in the Synthesis Stages of MCM-41-Type Mesoporous Molecular Sieves. *J. Phys. Chem. C* **2012**, *116*, 5376–5382. [[CrossRef](#)]
8. Lu, J.L.; Elam, J.W.; Stair, P.C. Synthesis and Stabilization of Supported Metal Catalysts by Atomic Layer Deposition. *Acc. Chem. Res.* **2013**, *46*, 1806–1815. [[CrossRef](#)] [[PubMed](#)]
9. Maki-Arvela, P.; Murzin, D.Y. Effect of catalyst synthesis parameters on the metal particle size. *Appl. Catal. A* **2012**, *451*, 251–281. [[CrossRef](#)]
10. Zhang, Y.; Liu, Y.; Yang, G.H.; Sun, S.L.; Tsubaki, N. Effects of impregnation solvent on Co/SiO₂ catalyst for Fischer-Tropsch synthesis: A highly active and stable catalyst with bimodal sized cobalt particles. *Appl. Catal. A* **2007**, *321*, 79–85. [[CrossRef](#)]
11. Li, Y.; Shen, W.J. Morphology-dependent nanocatalysts: Rod-shaped oxides. *Chem. Soc. Rev.* **2014**, *43*, 1543–1574. [[CrossRef](#)] [[PubMed](#)]
12. Shi, L.; Zeng, C.Y.; Lin, Q.H.; Lu, P.; Niu, W.Q.; Tsubaki, N. Citric acid assisted one-step synthesis of highly dispersed metallic Co/SiO₂ without further reduction: As-prepared Co/SiO₂ catalysts for Fischer-Tropsch synthesis. *Catal. Today* **2014**, *228*, 206–211. [[CrossRef](#)]
13. Zhu, Y.Y.; Wang, S.R.; Zhu, L.J.; Ge, X.L.; Li, X.B.; Luo, Z.Y. The influence of copper particle dispersion in Cu/SiO₂ catalysts on the hydrogenation synthesis of ethylene glycol. *Catal. Lett.* **2010**, *135*, 275–281. [[CrossRef](#)]
14. Qiu, S.B.; Zhang, X.; Liu, Q.Y.; Wang, T.J.; Zhang, Q.; Ma, L.L. A simple method to prepare highly active and dispersed Ni/MCM-41 catalysts by co-impregnation. *Catal. Commun.* **2013**, *42*, 73–78. [[CrossRef](#)]
15. Qiu, S.B.; Weng, Y.J.; Li, Y.P.; Ma, L.L.; Zhang, Q.; Wang, T.J. Promotion of Ni/MCM-41 Catalyst for Hydrogenation of Naphthalene by co-Impregnation with Polyols. *Chin. J. Chem. Phys.* **2014**, *27*, 433–438. [[CrossRef](#)]
16. Zhang, Y.J.; Bi, P.Y.; Wang, J.C.; Jiang, P.W.; Wu, X.P.; Xue, H.; Liu, J.X.; Zhou, X.G.; Li, Q.X. Production of jet and diesel biofuels from renewable lignocellulosic biomass. *Appl. Energy* **2015**, *150*, 128–137. [[CrossRef](#)]
17. De, S.; Saha, B.; Luque, R. Hydrodeoxygenation processes: Advances on catalytic transformations of biomass-derived platform chemicals into hydrocarbon fuels. *Bioresour. Technol.* **2015**, *178*, 108–118. [[CrossRef](#)] [[PubMed](#)]

18. Chen, G.Y.; Zhao, L.; Qi, Y. Enhancing the productivity of microalgae cultivated in wastewater toward biofuel production: A critical review. *Appl. Energy* **2015**, *137*, 282–291. [[CrossRef](#)]
19. Bi, P.Y.; Wang, J.C.; Zhang, Y.J.; Jiang, P.W.; Wu, X.P.; Liu, J.X.; Xue, H.; Wang, T.J.; Li, Q.X. From lignin to cycloparaffins and aromatics: Directional synthesis of jet and diesel fuel range biofuels using biomass. *Bioresour. Technol.* **2015**, *183*, 10–17. [[CrossRef](#)] [[PubMed](#)]
20. Hellinger, M.; Baier, S.; Mortensen, P.M.; Kleist, W.; Jensen, A.D.; Grunwaldt, J.D. Continuous Catalytic Hydrodeoxygenation of Guaiacol over Pt/SiO₂ and Pt/H-MFI-90. *Catalysts* **2015**, *5*, 1152–1166. [[CrossRef](#)]
21. Saidi, M.; Samimi, F.; Karimipourfard, D.; Nimmanwudipong, T.; Gates, B.C.; Rahimpour, M.R. Upgrading of lignin-derived bio-oils by catalytic hydrodeoxygenation. *Energy Environ. Sci.* **2014**, *7*, 103–129. [[CrossRef](#)]
22. Wang, H.M.; Male, J.; Wang, Y. Recent Advances in Hydrotreating of Pyrolysis Bio-Oil and Its Oxygen-Containing Model Compounds. *ACS Catal.* **2013**, *3*, 1047–1070. [[CrossRef](#)]
23. Hua, D.R.; Wu, Y.L.; Chen, Y.; Li, J.; Yang, M.D.; Lu, X.N. Co-Pyrolysis Behaviors of the Cotton Straw/PP Mixtures and Catalysis Hydrodeoxygenation of Co-Pyrolysis Products over Ni-Mo/Al₂O₃ Catalyst. *Catalysts* **2015**, *5*, 2085–2097. [[CrossRef](#)]
24. Mortensen, P.M.; Grunwaldt, J.D.; Jensen, P.A.; Knudsen, K.G.; Jensen, A.D. A review of catalytic upgrading of bio-oil to engine fuels. *Appl. Catal. A* **2011**, *407*, 1–19. [[CrossRef](#)]
25. Zhang, Q.; Jiang, T.; Li, B.; Wang, T.J.; Zhang, X.H.; Zhang, Q.; Ma, L.L. Highly Selective Sorbitol Hydrogenolysis to Liquid Alkanes over Ni/HZSM-5 Catalysts Modified with Pure Silica MCM-41. *ChemCatChem* **2012**, *4*, 1084–1087. [[CrossRef](#)]
26. Weng, Y.J.; Qiu, S.B.; Ma, L.L.; Liu, Q.Y.; Ding, M.Y.; Zhang, Q.; Zhang, Q.; Wang, T.J. Jet-Fuel Range Hydrocarbons from Biomass-Derived Sorbitol over Ni-HZSM-5/SBA-15 Catalyst. *Catalysts* **2015**, *5*, 2147–2160. [[CrossRef](#)]
27. Song, W.J.; Liu, Y.S.; Barath, E.; Zhao, C.; Lercher, J.A. Synergy effect of Ni and acid sites for C–O bond cleavage of phenol, catechol, and guaiacol. *Green Chem.* **2015**, *17*, 1204–1218. [[CrossRef](#)]
28. Hellinger, M.; Carvalho, H.W.P.; Baier, S.; Wang, D.; Kleist, W.; Grunwaldt, J.D. Catalytic hydrodeoxygenation of guaiacol over platinum supported on metal oxides and zeolites. *Appl. Catal. A* **2015**, *490*, 181–192. [[CrossRef](#)]
29. Lv, X.Y.; Chen, J.F.; Tan, Y.S.; Zhang, Y. A highly dispersed nickel supported catalyst for dry reforming of methane. *Catal. Commun.* **2012**, *20*, 6–11. [[CrossRef](#)]
30. Zhang, Q.; Wang, T.J.; Li, B.; Jiang, T.; Ma, L.L.; Zhang, X.H.; Liu, Q.Y. Aqueous phase reforming of sorbitol to bio-gasoline over Ni/HZSM-5 catalysts. *Appl. Energy* **2012**, *97*, 509–513. [[CrossRef](#)]
31. Wojcieszak, R.; Monteverdi, S.; Mercy, M.; Nowak, I.; Ziolek, M.; Bettahar, M.M. Nickel containing MCM-41 and AlMCM-41 mesoporous molecular sieves: Characteristics and activity in the hydrogenation of benzene. *Appl. Catal. A* **2004**, *268*, 241–253. [[CrossRef](#)]
32. Li, X.B.; Wang, S.R.; Cai, Q.J.; Zhu, L.J.; Yin, Q.Q.; Luo, Z.Y. Effects of Preparation Method on the Performance of Ni/Al₂O₃ Catalysts for Hydrogen Production by Bio-Oil Steam Reforming. *Appl. Biochem. Biotech.* **2012**, *168*, 10–20. [[CrossRef](#)] [[PubMed](#)]
33. Moya, S.F.; Martins, R.L.; Schmal, M. Monodispersed and nanostructured Ni/SiO₂ catalyst and its activity for non oxidative methane activation. *Appl. Catal. A* **2011**, *396*, 159–169. [[CrossRef](#)]
34. Dutta, D.; Borah, B.J.; Saikia, L.; Pathak, M.G.; Sengupta, P.; Dutta, D.K. Synthesis and catalytic activity of Ni-acid activated montmorillonite nanoparticles. *Appl. Clay Sci.* **2011**, *53*, 650–656. [[CrossRef](#)]
35. Ren, H.P.; Hao, Q.Q.; Wang, W.; Song, Y.H.; Cheng, J.; Liu, Z.W.; Liu, Z.T.; Lu, J.; Hao, Z.P. High-performance Ni-SiO₂ for pressurized carbon dioxide reforming of methane. *Int. J. Hydrog. Energy* **2014**, *39*, 11592–11605. [[CrossRef](#)]
36. Kirumakki, S.R.; Shpeizer, B.G.; Sagar, G.V.; Chary, K.V.R.; Clearfield, A. Hydrogenation of naphthalene over NiO/SiO₂-Al₂O₃ catalysts: Structure-activity correlation. *J. Catal.* **2006**, *242*, 319–331. [[CrossRef](#)]
37. Fang, K.G.; Ren, J.; Sun, Y.H. Effect of nickel precursors on the performance of Ni/AlMCM-41 catalysts for *n*-dodecane hydroconversion. *J. Mol. Catal. A Chem.* **2005**, *229*, 51–58. [[CrossRef](#)]
38. Chao, K.J.; Chiou, B.H.; Cho, C.C.; Jeng, S.Y. Temperature-programmed desorption studies on ZSM-5 zeolites. *Zeolites* **1984**, *4*, 2–4. [[CrossRef](#)]
39. Lobree, L.J.; Hwang, I.C.; Reimer, J.A.; Bell, A.T. Investigations of the State of Fe in H-ZSM-5. *J. Catal.* **1999**, *186*, 242–253. [[CrossRef](#)]

40. Yang, Y.X.; Ochoa-Hernandez, C.; O'Shea, V.A.D.; Pizarro, P.; Coronado, J.M.; Serrano, D.P. Effect of metal-support interaction on the selective hydrodeoxygenation of anisole to aromatics over Ni-based catalysts. *Appl. Catal. B* **2014**, *145*, 91–100. [[CrossRef](#)]
41. Li, X.M.; Han, D.Z.; Wang, H.; Liu, G.B.; Wang, B.; Li, Z.; Wu, J.H. Propene oligomerization to high-quality liquid fuels over Ni/HZSM-5. *Fuel* **2015**, *144*, 9–14. [[CrossRef](#)]
42. Van der Borght, K.; Galvita, V.V.; Marin, G.B. Reprint of "Ethanol to higher hydrocarbons over Ni, Ga, Fe-modified ZSM-5: Effect of metal content". *Appl. Catal. A* **2015**, *504*, 621–630. [[CrossRef](#)]
43. Yu, M.J.; Park, S.H.; Jeon, J.K.; Ryu, C.; Sohn, J.M.; Kim, S.C.; Park, Y.K. Hydrodeoxygenation of Guaiacol Over Pt/Al-SBA-15 Catalysts. *J. Nanosci. Nanotechnol.* **2015**, *15*, 527–531. [[CrossRef](#)] [[PubMed](#)]
44. Hong, Y.K.; Lee, D.W.; Eom, H.J.; Lee, K.Y. The catalytic activity of Pd/WO_x/gamma-Al₂O₃ for hydrodeoxygenation of guaiacol. *Appl. Catal. B* **2014**, *150*, 438–445. [[CrossRef](#)]
45. Nimmanwudipong, T.; Runnebaum, R.C.; Block, D.E.; Gates, B.C. Catalytic Conversion of Guaiacol Catalyzed by Platinum Supported on Alumina: Reaction Network Including Hydrodeoxygenation Reactions. *Energy Fuel* **2011**, *25*, 3417–3427. [[CrossRef](#)]



© 2016 by the authors; licensee MDPI, Basel, Switzerland. This article is an open access article distributed under the terms and conditions of the Creative Commons Attribution (CC-BY) license (<http://creativecommons.org/licenses/by/4.0/>).